

Geophysical Research Letters[®]



RESEARCH LETTER

10.1029/2024GL109793

Key Points:

- A machine learning potential of ab initio quality is developed for the Mg-Fe-O system
- Mg exsolves in the form of crystalline Fe-poor ferropericlase with a small exsolution rate assuming only Mg and O are present in the core
- MgO exsolution may serve as an important source of buoyant flux to drive the early geodynamo

Supporting Information:

Supporting Information may be found in the online version of this article.

Correspondence to:

J. Deng,
jie.deng@princeton.edu

Citation:

Deng, J. (2024). Large-scale atomistic simulations of magnesium oxide exsolution driven by machine learning potentials: Implications for the early geodynamo. *Geophysical Research Letters*, 51, e2024GL109793. <https://doi.org/10.1029/2024GL109793>

Received 13 APR 2024

Accepted 5 AUG 2024

Large-Scale Atomistic Simulations of Magnesium Oxide Exsolution Driven by Machine Learning Potentials: Implications for the Early Geodynamo

Jie Deng¹ 

¹Department of Geosciences, Princeton University, Princeton, NJ, USA

Abstract The precipitation of magnesium oxide (MgO) from the Earth's core has been proposed as a potential energy source to power the geodynamo prior to the inner core solidification. Yet, the stable phase and exact amount of MgO exsolution remain elusive. Here we utilize an iterative learning scheme to develop a unified deep learning interatomic potential for the Mg-Fe-O system valid over a wide pressure-temperature range. This potential enables direct, large-scale simulations of MgO exsolution processes at the Earth's core-mantle boundary. Our results suggest that Mg exsolves in the form of crystalline Fe-poor ferropericlase as opposed to a liquid MgO component presumed previously. The solubility of Mg in the core is limited, and the present-day core is nearly Mg-free. The resulting exsolution rate is small yet nonnegligible, suggesting that MgO exsolution may provide a potentially important energy source, although it alone may be difficult to drive an early geodynamo.

Plain Language Summary The paleomagnetic records suggest that Earth's magnetic field dates back to at least 3.4 billion years ago. Yet, the energy source of this early geodynamo is still puzzling. One popular hypothesis is that buoyant magnesium oxide may exsolve out of the Earth's core as the core cools, releasing gravitational potential energy to drive the core convection and power the early geodynamo. However, the amount of MgO exsolved is uncertain due to experimental and computational challenges. Here, for the first time, we directly simulate the MgO exsolution processes using large-scale molecular dynamics simulations, made possible by interatomic potentials built upon machine learning methods. The results show that MgO exsolves as a component of a crystalline ferropericlase, in contrast to early studies which generally assume that MgO exsolved as a component of silicate melts. We find that MgO solubility in the core is low. The exsolution rate is small and MgO alone may be insufficient to sustain a long-lasting magnetic field at the Earth's surface in its early history.

1. Introduction

Chemical buoyancy due to the crystallization of the inner core is believed to have supplied energy to power the geodynamo in the last 0.5–1 billion years (Nimmo, 2015). Paleomagnetic records suggest the existence of a very early (3.4 Ga) magnetic field in the Earth's history prior to the inner core crystallization (Tarduno et al., 2010). The energy source of this early geodynamo is enigmatic. Radiogenic heat production in the core may not be sufficient to sustain an early dynamo (D. A. Frost et al., 2022). The basal magma ocean may be electrically conductive (Stixrude et al., 2020), but the conductivity, scale, and longevity of a convective basal magma ocean are uncertain (Okuda et al., 2024).

Recent studies propose that exsolution of oxides from the core upon cooling, such as MgO (O'Rourke & Stevenson, 2016) or SiO₂ (Hirose et al., 2017), may be a viable mechanism to power an early dynamo. Experimental studies on metal-silicate partitioning suggest that the solubility of Mg is highly sensitive to temperature (James Badro et al., 2016; Du et al., 2017). The high-temperature equilibration between the metallic and silicate melts during the core formation process may result in a few wt% of MgO dissolved in the core. Upon cooling, Mg is expected to precipitate out of the core as its solubility drops. However, the efficiency of this mechanism, especially for MgO oxide, remains controversial (James Badro et al., 2016; Du et al., 2017).

The precipitation rate of MgO has been widely estimated using Mg partitioning behaviors in the metal-silicate system (James Badro et al., 2018; Du, Boujibar, et al., 2019; Liu et al., 2019). This estimation applies when the core fluid is directly in contact with silicate melts, assuming that either the lowermost mantle is molten or the

© 2024. The Author(s).

This is an open access article under the terms of the [Creative Commons](#)

[Attribution License](#), which permits use, distribution and reproduction in any medium, provided the original work is properly cited.

exsolved phase is silicate melt. However, the core-mantle interface is complex, and the exact phase of precipitation depends on bulk core compositions and thermodynamic conditions, which are still under debate (Christopher J. Davies & Greenwood, 2023; Helffrich et al., 2020). Indeed, Si may exsolve as SiO_2 solid (Hirose et al., 2017). Likewise, if the lowermost mantle in contact with the core and the initial core is silicon depleted, Mg may exsolve out of the core in solid-state given its highly refractory nature (Alfè, 2005; Du & Lee, 2014). Therefore, a careful examination of the Mg exsolution process is necessary.

In this study, we combine enhanced sampling, feature selection, and deep learning to develop a unified machine learning potential (MLP) for the Mg-Fe-O system. This MLP is used to perform large-scale molecular dynamics simulations to study the exsolution of Mg from core fluids. Unlike previous computational studies based on free energy calculations (C. J. Davies et al., 2018; Wahl & Militzer, 2015; Wilson et al., 2023), this method does not prescribe the state of the exsolved phase. The results inform the stable state of MgO precipitation, Mg and O partitioning between core fluid and exsolution, and the efficiency of MgO exsolution in powering an early geodynamo.

2. Methodology

2.1. Development of Machine Learning Potential

A machine learning potential (MLP) is a non-parametric model that approximates the Born-Oppenheimer potential energy surface. We follow the same approaches outlined in our previous work on Mg-Si-O (Deng et al., 2023) and Mg-Si-O-H (Peng & Deng, 2024), where details of the machine learning process can be found. To briefly summarize, the MLP is trained on a set of configurations drawn from multithermal and multibaric (MTMP) simulations (Piaggi & Parrinello, 2019), which efficiently sample the multi-phase configuration space. We use the structure factor of B1 MgO as the collective variable to drive the sampling, and an iterative learning scheme as described by Deng et al. (2023) to select distinct samples from molecular dynamics trajectories efficiently.

High-accuracy ab initio calculations are performed on the selected sample configurations to derive the corresponding energies, atomic forces, and stresses. The DeePMD approach is employed to train an MLP that takes a configuration (a structure of a given atomic arrangement) and predicts its energy, atomic forces, and stresses without iterating through the time-consuming self-consistent field calculation (Wang et al., 2018; Zhang et al., 2018). The details of DeePMD approach and density functional theory (DFT) calculations can be found at Supplementary Information (Text S1, Figure S1 in Supporting Information S1). Our MLP explores a wide compositional space, trained on Mg-Fe-O systems of varying Mg:Fe:O ratios, including the pure endmembers, Fe and MgO , as well as intermediate compositions denoted by $(\text{MgO})_a\text{Fe}_b\text{O}_c$, where $a = 0-64$, $b = 0-64$, $c = 0-16$ with $2a + b \geq 64$. The final training set consists of 4,466 configurations generated at pressures up to 200 GPa and temperatures up to 8000 K.

2.2. Two-Phase Molecular Dynamics Simulation

Two-phase simulations are performed on a pure MgO system to determine the melting point of B1 MgO . Alfè (2005) found that systems of 432 atoms are sufficient to yield converged melting points comparable to those larger systems. Here, supercells of 432 atoms are constructed and then relaxed for 1,000 steps at desired pressure and temperature conditions in the NPT ensemble. The relaxed cell is then used to perform NVT simulations at high temperatures far exceeding the melting temperatures, with the atoms of half the cell fixed and the force applied to these atoms set to zero. The resulting structure is half-molten and half-crystalline. The structure is then relaxed again at the target pressure and temperature for 1,000 steps to obtain the initial configuration for two-phase simulations. Simulations on the two-phase supercell of solid-liquid coexistence were then performed. If the whole cell is molten (or crystallized) at the end, the simulation temperature is above (or below) the melting point. The state of the system is determined by analyzing the radial distribution functions, allowing us to pinpoint the upper and lower bounds of the melting point.

2.3. Exsolution Simulation

We construct systems of various Mg:Fe:O ratios by substituting or removing Mg and/or O atoms of supercells of B1 MgO . Initial configurations are melted at 8000 K and 140 GPa under the NPT ensemble for approximately

10 ps. Trajectories and radial distribution functions are inspected to ensure systems are fully molten and well relaxed. The resulting configurations are further used to perform simulations at 140 GPa and target temperatures under the NPT ensemble for up to several nanoseconds to simulate the exsolution process. We use the Gibbs dividing surface method to determine the composition of the two coexisting phases of the simulation results (Text S1 in Supporting Information [S1](#)).

3. Results and Discussion

3.1. Benchmarks of the Machine Learning Potential

We compare the energies, atomic forces, and stresses from the MLP to those from DFT calculations for 15,078 configurations that are not included in the training set (Figure S2 in Supporting Information [S1](#)). The root-mean-square errors of the energies, atomic forces, and stresses are 6.34 meV/atom⁻¹, 0.27 eV/Å⁻¹, and 0.48 GPa, respectively.

We perform two additional tests to further examine the reliability of the MLP. First, we perform MD simulations with supercells of B1 MgO solid, MgO liquid, and a Mg-Fe-O liquid mixture. These supercells are larger than the training configurations. The root-mean-square error of energy prediction by the MLP with respect to the DFT calculations is similar to the error in the testing sets (Figure S3 in Supporting Information [S1](#)). This verification test further proves the accuracy of energy prediction and [demonstrated](#) the transferability of the MLP to structures larger than the training/testing sets. Second, we calculate the melting point of B1 MgO at 140 GPa using the solid-liquid two-phase coexistence method with a supercell of 432 atoms. For both DFT and MLP, the system crystallizes at 7700 K and melts at 7800 K, suggesting a melting point of $7,750 \pm 50$ K at 140 GPa, further validating the robustness of the MLP. The melting temperature is also consistent with previous studies (Alfè, 2005; Du & Lee, 2014).

3.2. System Convergence of the Exsolution Simulation

The robust MLP of the Mg-Fe-O system allows for large-scale exsolution simulations. We first examine the convergence of Fe liquid composition with respect to the simulation cell size by performing exsolution simulations at 5000 K and 140 GPa with five Mg-Fe-O liquid mixtures, where the ratios of Mg, O and Fe atoms are fixed as 2:2:3, that is, $Mg_{64}O_{64}Fe_{96}$, $Mg_{512}O_{512}Fe_{768}$, $Mg_{1728}O_{1728}Fe_{2592}$, $Mg_{2304}O_{2304}Fe_{3456}$, $Mg_{3136}O_{3136}Fe_{4704}$. In all simulation, the system quickly demixes to form MgO-rich and Fe-rich regions, and subsequently, the MgO-rich region spontaneously crystallizes to form ferropericlase while metallic phase remains liquid. The resulting atomic fractions of Mg, O in the metallic phase converge when the system size reaches 2,000 atoms (Figure S4 in Supporting Information [S1](#)). Large systems also yield better statistics and thus the smaller uncertainties in the atomic fraction. Based on this test, all the partitioning results reported here are derived from simulations performed with systems of more than 2,000 atoms to ensure convergence and robust statistics.

3.3. Exsolution Process

In all simulations considered, exsolution spontaneously occurs within a few picoseconds at 4000 K to a few nanoseconds at 5500 K. The exsolved phase are all solid ferropericlase with small amounts of FeO. The interfaces between exsolution and Fe liquid are typically irregular as they form spontaneously without interference. Taking the exsolution simulation of $Mg_{208}Fe_{3456}O_{2520}$ liquid at 140 GPa and 5500 K as an example (Figure 1; Supplementary movie 1), it starts with a homogeneous liquid (Figure 1a), and quickly demixes to form patches of MgO-rich liquid and Fe-rich liquid with a continuous drop of potential energy. Within around 250 ps, MgO-rich patches and Fe-rich patches conglomerate, respectively, dividing the whole cell into two regions: one enriched in MgO and the other Fe. The MgO-rich region remains liquid for another 750 ps until a sudden crystallization occurs to form ferropericlase (Figure 1b). The crystallization is a rapid process accompanied by a significant drop in potential energy. Quickly after ferropericlase crystallizes, the potential energy plateaus. The element exchange between ferropericlase and residual Fe liquid continues within the interface region. We analyze the trajectories at this stage, calculate the Gibbs dividing surface, and determine the average composition of each phase for the last 100 ps. The chemical compositions of both phases are shown in Figure 1c. The metallic liquid is oxygen rich and magnesium poor. The exsolved ferropericlase is of B1 structure and is nearly stoichiometric ($Mg_{0.974}Fe_{0.026}O$). Similar analyses have been applied to all other exsolution simulations, and the compositions of simulation products are summarized in Table S1 in Supporting Information [S1](#).

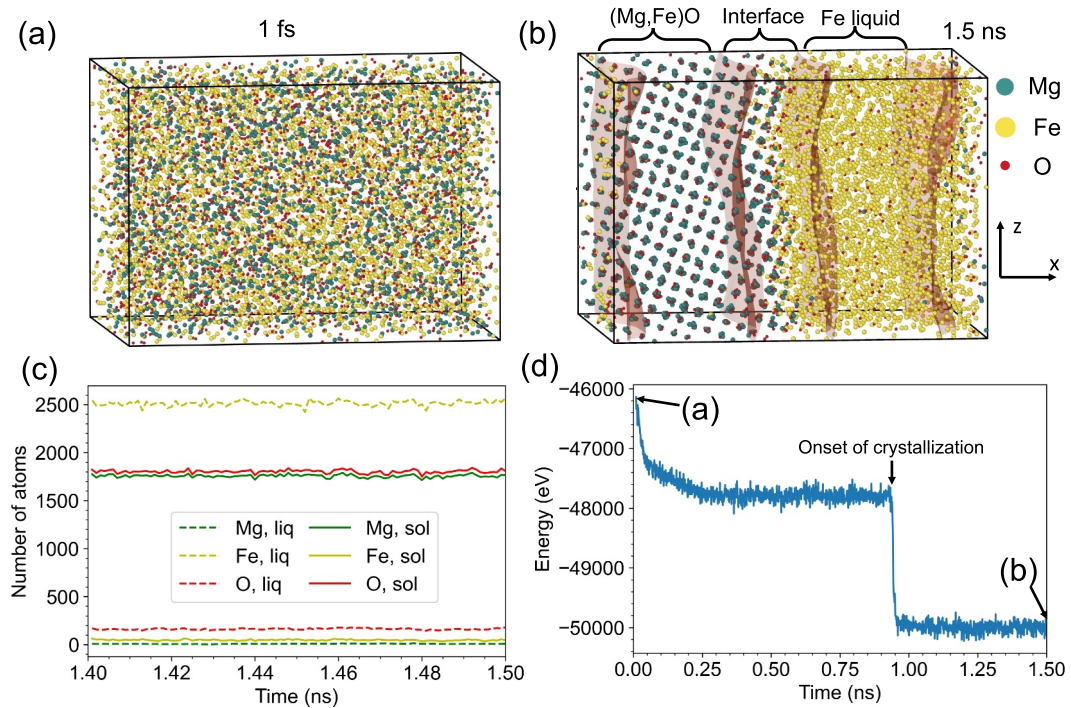


Figure 1. Molecular dynamics simulation of spontaneous ferropericlase exsolution from a homogeneous $\text{Mg}_{2088}\text{Fe}_{3456}\text{O}_{2520}$ liquid at 140 GPa and 5500 K (NPT ensemble). (a) The initial configuration at 1 fs with a homogeneous distribution of Mg (green), Fe (yellow), and O (red) atoms. (b) The final configuration at 1.5 ns. Dark red planes are the Gibbs dividing surfaces that separate the whole systems into crystalline ferropericlase, interface, and metallic liquid. The cell dimension is $50.9 \text{ \AA} \times 39.9 \text{ \AA} \times 35.3 \text{ \AA}$ initially (a) and becomes $47.9 \text{ \AA} \times 37.6 \text{ \AA} \times 33.3 \text{ \AA}$ at the end of the simulation (b). (c) Evolution of number of atoms in liquid (liq) and solid exsolution (sol) in the last 100 ps. (d) Evolution of potential energy. Energy drops with the separation of ferropericlase and metallic liquid. The sudden drop of internal energy corresponds to the crystallization of ferropericlase.

3.4. Element Partitioning

We further analyze the element partitioning between the exsolved ferropericlase and Fe liquid considering two dissociation reactions: $\text{MgO}^{\text{ox}} = \text{Mg}^{\text{met}} + \text{O}^{\text{met}}$ and $\text{FeO}^{\text{ox}} = \text{Fe}^{\text{met}} + \text{O}^{\text{met}}$, where superscripts *ox* and *met* indicate oxide and metal, respectively. We also consider Mg exchange reaction with $\text{MgO}^{\text{ox}} + \text{Fe}^{\text{met}} = \text{FeO}^{\text{ox}} + \text{Mg}^{\text{met}}$, but the fit is poor, as also reported in other studies (James Badro et al., 2018; Liu et al., 2019). The exchange coefficients for Mg ($K_D^{\text{Mg}} = X_{\text{Mg}}^{\text{met}} X_{\text{O}}^{\text{met}} / X_{\text{MgO}}^{\text{ox}}$) and O ($K_D^{\text{O}} = X_{\text{Fe}}^{\text{met}} X_{\text{O}}^{\text{met}} / X_{\text{FeO}}^{\text{ox}}$) are summarized in Figure 2, where X_i^k is the molar fraction of element *i* in phase *k*. Both K_D^{Mg} and K_D^{O} increase with temperature and oxygen concentration in the metallic liquid. K_D^{Mg} and K_D^{O} are fitted simultaneously to a standard thermodynamic model with the non-ideality described by the epsilon formalism of (Ma, 2001). The phase relation between ferropericlase and Fe liquid has been studied mostly at low pressures and low temperatures (Asahara et al., 2007; D. J. Frost et al., 2010; Ozawa et al., 2008). Unfortunately, Mg contents in metallic melts were not reported, and only K_D^{O} were reported in these studies. Thus, we only include K_D^{O} of these experiments in the fitting (Texts S2, S3 in Supporting Information S1; Tables S2 in Supporting Information S2).

Our calculated K_D^{Mg} is slightly larger than that reported by a recent ab initio calculation (Wilson et al., 2023) where the pure B1 MgO is assumed as the exsolved phase, while our exsolution simulations show that precipitates contain small amounts of FeO (Figure 1, Table S1 in Supporting Information S1). The incorporation of FeO in the exsolved phase likely changes the free energy of the system, leading to differences in K_D^{Mg} . Nevertheless, the good agreement of K_D^{Mg} by these two studies is remarkable given that they employed completely different methods—free energy method by Wilson et al. (2023) versus direct MD simulation here—and considered very different system size—a few hundred atoms by Wilson et al. (2023) versus a few thousand atoms here. Wahl and Miller (2015) also performed ab initio simulations on the Mg-Fe-O system but focus on high temperatures close to

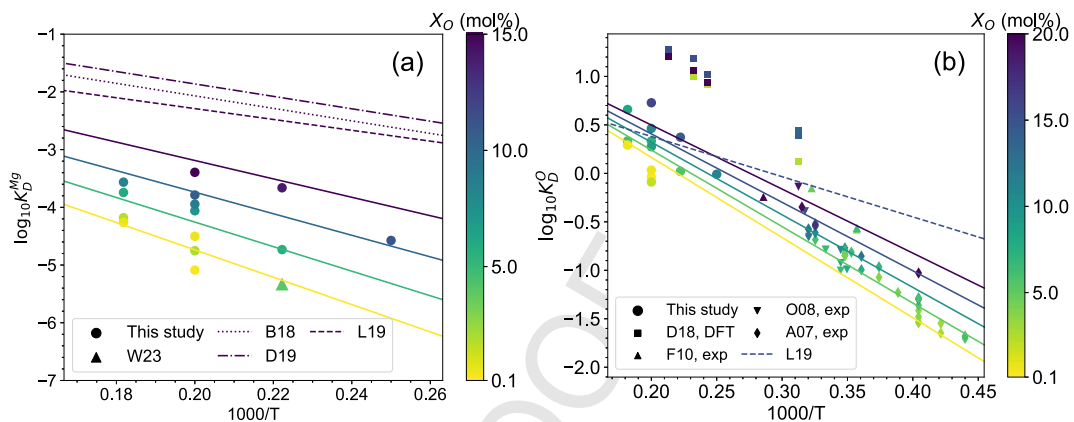


Figure 2. Mg (a) and O (b) exchange coefficients as a function of oxygen content in the iron (X_O) and temperature at 140 GPa. Solid circles are the results from this study, and solid lines are the best-fit curves (Supplementary Texts S2, S3 in Supporting Information S1). The color of curves and symbols represents the value of X_O . Previous calculations and experiments are also shown for comparison. (a) W23 denotes the DFT calculation result by (Wilson et al., 2023) (upward triangle). B18 (dotted line), L19 (dashed line), and D19 (dotted-dashed line) represents the Mg exchange coefficient between silicate melt and Fe liquid calibrated by (James Badro et al., 2018; Liu et al., 2019; Du, Boujibar, et al., 2019), respectively. (b) Experimental studies include (Ozawa et al., 2008) (O08, downward triangle) (Asahara et al., 2007), (A07, diamond) (D. J. Frost et al., 2010), (F10, upward triangle). DFT study includes (C. J. Davies et al., 2018) (D18, square). All previous results are normalized to 140 GPa for a direct comparison using the best-fit pressure dependence,

$$\log_{10} K_D^O(140 \text{ GPa}) = \log_{10} K_D^O(\text{experiment}) - \frac{c_O(140-P)}{T}$$

where P/T are experimental/calculation pressure/temperature, and c_O is a fitted constant (Table S3 in Supporting Information S1). L19 (dashed line) indicates the O exchange coefficient of silicate-melt calibrated by (Liu et al., 2019). Uncertainties of the exchange coefficients of this study are roughly represented by the symbol size.

the solvus closure and did not report Mg partitioning results at the conditions overlapping this study, which precludes a direct comparison. Compared with the previously determined K_D^{Mg} between Fe liquid and silicate melt (James Badro et al., 2018; Du, Boujibar, et al., 2019; Liu et al., 2019), K_D^{Mg} between Fe liquid and solid ferropericlase shows similar temperature dependence but is overall approximately one order of magnitude lower (Figure 2a), indicating a low Mg content in Fe liquid when equilibrated with ferropericlase. This is expected as MgO preferentially enters ferropericlase when silicate melt crystallizes (Boukaré et al., 2015).

Oxygen partitioning between ferropericlase and liquid Fe is strongly controlled by temperature, in agreement with previous experiments (Asahara et al., 2007; D. J. Frost et al., 2010; Ozawa et al., 2008) and calculations (C. J. Davies et al., 2018). K_D^O between Fe liquid and silicate melt derived by (Liu et al., 2019) generally aligns with K_D^O between Fe liquid and solid ferropericlase, especially at high temperatures. Our K_D^O can be well fitted with previous experimental data to a unified thermodynamic model (Asahara et al., 2007; Ozawa et al., 2008), except for the four data points reported by (D. J. Frost et al., 2010) (Text S3; Table S3 in Supporting Information S1). At around 30–70 GPa and with similar oxygen contents in the liquid Fe, K_D^O of (D. J. Frost et al., 2010) are around half log unit higher than those of (Ozawa et al., 2008) and our extrapolated results. The source of this discrepancy is unknown but may arise from the carbon contamination. K_D^O reported by an early DFT calculation (C. J. Davies et al., 2018) is around 0.3–0.6 log unit higher than those of (Ozawa et al., 2008) and our results at similar conditions. We note that C. J. Davies et al. (2018) calculated the chemical potential of FeO for defect-free (Mg,Fe)O. Yet, both our simulations and previous studies (B. B. Karki & Khanduja, 2006; Van Orman et al., 2003) support the existence of defects in ferropericlase at high temperatures, which may lower the free energy of the host mineral and enrich FeO in ferropericlase, leading to a reduced K_D^O .

4. Exsolution Rate and Geodynamo

Earth's accretion and differentiation in its early history likely resulted in a core much hotter than it is today. The precipitation of light elements due to the secular cooling of the core may have provided a vital energy source to drive the geodynamo. The energetics of the exsolution-powered dynamo hinge on the cooling rate and the exsolution rate. Here, we adopt a core thermal evolution model proposed by (O'Rourke & Stevenson, 2016), with

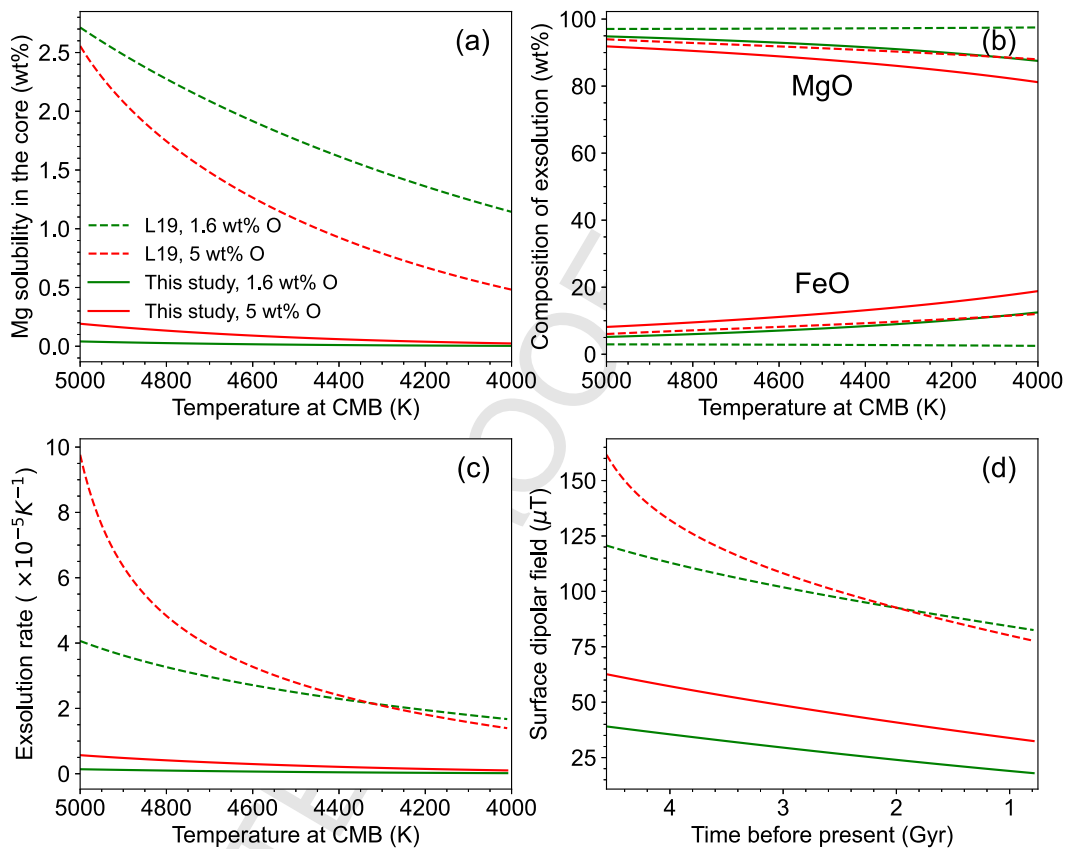


Figure 3. MgO solubility (a), chemical composition of the exsolution (b), exsolution rate (c), intensity of the dipolar magnetic field at Earth's surface produced by exsolution-driven dynamo (d) based on the element partitioning models from this study with crystalline ferropericlase as the exsolved phase (solid lines) and those from a recent study with silicate melts as the exsolved phase (dashed lines) (Liu et al., 2019), respectively. Red and green denote initial oxygen concentration in the core of 5 wt% and 1.6 wt% at 5000 K, respectively.

which the composition of exsolution and the associated exsolution rate can be further determined using the element partitioning models (Text S4 in Supporting Information S1). All previous modeling of Mg exsolution from the core assume that MgO exsolve as a component of silicate melts. However, our simulations show that MgO exsolves as a component of crystalline ferropericlase, at least when light elements other than Mg and O are absent. Here, we first examine the Mg exsolution and its potential to drive the early geodynamo for an Mg- and O-bearing core, and then we discuss the effects of additional light elements.

To model Mg exsolution from a core fluid with only Mg and O as light elements, we first determine the saturation conditions under which Mg precipitates. Previous N-body simulations and metal-silicate equilibrium experiments suggest that the Earth's core following its formation may contain 1.6–5 wt% O (Fischer et al., 2017; Liu et al., 2019; Rubie et al., 2015). The corresponding saturation magnesium concentration in the core is 0.04–0.19 wt% at 140 GPa, as determined using the K_D^{Mg} between metal and ferropericlase, which is significantly lower than that determined by K_D^{Mg} between metal and silicate melt (Liu et al., 2019) (Figure 3a). This difference is expected, as the former K_D^{Mg} value is about one order of magnitude smaller than the latter (Figure 2a). Hence, our work implies that a substantial amount of Mg may have already been exsolved by the time the core cools to a CMB temperature (T_{CMB}) of 5000 K. Further cooling reduces the Mg solubility in the core, with concentrations approaching 0.02–0.003 wt% at a T_{CMB} of 4000 K. This suggests a diminishingly small amount of Mg in the present-day outer core. We use these saturation magnesium conditions as the initial core composition in our exsolution modeling.

Despite the contrasting Mg solubilities in the core, the compositions of the precipitations are similar and exhibit a comparable trend with temperature. Specifically, the exsolved phase in both models becomes increasingly FeO-

rich with cooling. At 4000 K, the exsolution contains up to 20 wt% FeO (Figure 3b). Throughout the thermal history, T_{CMB} is lower than the solidus of exsolved ferropericlase (Deng et al., 2019), indicating that precipitations remain solid.

The resulting exsolution rates decrease with temperature, with the values dropping from $1.4 \times 10^{-6} \text{ K}^{-1}$ at 5000 K to $0.2-1.0 \times 10^{-6} \text{ K}^{-1}$ at 4000 K. Exsolution rates of ferropericlase are approximately one order of magnitude smaller than those predicted for silicate melt exsolution (Figure 3c). The precipitated phase is depleted in iron and enriched in Mg. As a result, they are lighter than the outer core fluid. It is generally assumed that precipitation occurs near the CMB (Hirose et al., 2017; O'Rourke & Stevenson, 2016), leading to a change in the overall density profile of the compositionally well-mixed liquid core. The gravitational potential energy released by this process may sustain an exsolution-driven dynamo. Converting the exsolution rate to the magnetic field intensity is model dependent, however. The upper bound of the exsolution rates ($1-5.6 \times 10^{-6} \text{ K}^{-1}$) derived here are similar to the previous reports (James Badro et al., 2016; Du et al., 2017). While Du, Boujibar, et al. (2019) conclude that this exsolution rate is not sufficient to power the early geodynamo alone, James Badro et al. (2018) use a scaling law that relates the exsolution rate to dipolar magnetic field intensity ($B_{\text{surface}}^{\text{dipole}}$) and argue that MgO exsolution can well produce the dipolar magnetic field intensity at Earth's surface consistent with observations. We follow (James Badro et al., 2018) to convert the exsolution rate to $B_{\text{surface}}^{\text{dipole}}$ (Figure 3d). The results show that $B_{\text{surface}}^{\text{dipole}}$ generated by the upper bound exsolution rate is broadly consistent with the paleo-intensities records dating back to 3.4 Gyr (Tarduno et al., 2010), and that generated by the lower bound rate is overall smaller than the observations and thus may not be sufficient (Tarduno et al., 2015). Overall, we find that MgO exsolution alone may be difficult to power the early geodynamo, but it is nevertheless an important energy source.

While the exact composition of the core remains unknown, it may contain other light elements, such as S, Si, C, and H (Hirose et al., 2021). As the core cools, the solubility of these light elements tends to decrease, leading to their exsolution. For example, in a core composed solely of Si, O, and Fe, the exsolved phase would likely be solid SiO_2 (Hirose et al., 2017). The study by Helffrich et al. (2020) on the joint solubility of Mg, O, and Si in liquid Fe suggests that the presence of Si enhances the retention of Mg in metal, thereby reducing the extent of MgO exsolution. It is crucial to note, however, that their thermodynamic model is based on data from the silicate melt-Fe system and the SiO_2 -Fe system without considering ferropericlase. As a result, in their model, MgO is implicitly treated as a component of liquid rather than as solid ferropericlase. Adding further complexity, instead of precipitating separate MgO and SiO_2 solids, a Mg-Fe-Si-O system may yield exsolution of MgSiO_3 bridgemanite or post-perovskite. Indeed, bridgemanite and post-perovskite with low iron content are quite refractory, with melting temperatures exceeding the T_{CMB} assumed here and thus may form stable exsolution phases (Deng et al., 2023). Whether bridgemanite, post-perovskite, solid SiO_2 , B1 MgO, or liquid is the stable exsolution phase depends on their free energies and is still open to question. If multiple phases precipitate simultaneously, the Mg exsolution rate is orders of magnitude higher for silicate melt exsolution than for ferropericlase exsolution. In this case, the ferropericlase exsolution would be insignificant in transporting Mg and driving the geodynamo compared with silicate melt exsolution, as suggested by (Wilson et al., 2023). Consequently, a comprehensive re-evaluation of the phase relations in the Mg-Si-O-Fe system and more broadly, in the Mg-Si-O-C-H-S-Fe system, which considers exsolution as solids, is warranted. This study marks a first attempt to demonstrate the significance of solid exsolution and the substantially different behaviors they exhibit during exsolution.

5. Conclusion

We developed a machine learning potential of ab initio quality for Mg-Fe-O system using the iterative training scheme, enabling large-scale atomistic simulations of Mg exsolution processes at 4,000–5500 K and 140 GPa without any ad hoc assumptions regarding the stable exsolution phase. The exsolved phase is solid Fe-poor ferropericlase across all the thermodynamic conditions considered. Using the Gibbs dividing surface method, we analyze simulation trajectories, obtain the chemical composition of exsolved phases and liquid phases, and determine Mg and O exchange coefficients. The results show that partitioning of Mg into the exsolved phase is significantly enhanced when compared to scenarios where the exsolved phase is assumed to be liquid, as in previous studies (James Badro et al., 2018; Du, Boujibar, et al., 2019; Liu et al., 2019; Mittal et al., 2020). The resulting small Mg exchange coefficients suggest a reduced Mg solubility in the core. Assuming a reasonable initial core composition with 1.6–5 wt% oxygen, the MgO exsolution rate may be insufficient to generate the dipolar magnetic field at the Earth's surface with intensities that align with the paleomagnetic record.

Though not the focus of this study, it is noteworthy that our oxygen exchange coefficients are smaller than the previous ab initio results, indicating a reduced transport of FeO from ferropericlase into the core fluid (C. J. Davies et al., 2018), with implications for the dynamics of long-term core–mantle interaction. Moreover, solid exsolution may encapsulate distinctive core–characteristic signatures and transport them into certain regions of the overlaying mantle (Helffrich et al., 2018), offering a valuable window to probe the core–mantle interaction (Deng & Du, 2023).

Data Availability Statement

All the data used in this study are stored at the Open Science Framework via DOI 10.17605/OSF.IO/MSRV4 (Deng, 2024). For the software packages used in this study, Vienna Ab initio Simulation Package (VASP) (Kresse & Furthmüller, 1996), LAMMPS Release 15 September 2022 (Plimpton et al., 2022), PLUMED 2 (Bonomi et al., 2019), and DeePMD-kit v2.1.5 (Zeng et al., 2023) were used.

Badro, 2014; Deng and Stixrude, 2021a; Deng and Stixrude, 2021b; Fischer et al., 2015; Holmström and Stixrude, 2015; Hoover, 1985; Hornik et al., 1989; Karki et al., 2018; Korell et al., 2019; Kresse and Joubert, 1999; Lorenz et al., 2004; Mermin, 1965; Perdew et al., 2008; Scipioni et al., 2017; Segà et al., 2018; Willard and Chandler, 2010; Xiao and Stixrude, 2018.

Acknowledgments

This work was funded by the National Science Foundation under Grant EAR-2242946. The simulations presented in this article were performed on computational resources managed and supported by Princeton Research Computing, a consortium of groups including the Princeton Institute for Computational Science and Engineering (PICSciE) and the Office of Information Technology's High-Performance Computing Center and Visualization Laboratory at Princeton University.

References

Alfè, D. (2005). Melting curve of MgO from first-principles simulations. *Physical Review Letters*, 94(23), 235701. <https://doi.org/10.1103/PhysRevLett.94.235701>

Asahara, Y., Frost, D. J., & Rubie, D. C. (2007). Partitioning of FeO between magnesiowustite and liquid iron at high pressures and temperatures: Implications for the composition of the Earth's outer core. *Earth and Planetary Science Letters*, 257(3–4), 435–449. <https://doi.org/10.1016/j.epsl.2007.03.006>

Badro, J. (2014). Spin transitions in mantle minerals. *Annual Review of Earth and Planetary Sciences*, 42(42), 231–248. <https://doi.org/10.1146/annurev-earth-042711-105304>

Badro, J., Aubert, J., Hirose, K., Nomura, R., Blanchard, I., Borensztajn, S., & Siebert, J. (2018). Magnesium partitioning between Earth's mantle and core and its potential to drive an early exsolution geodynamo. *Geophysical Research Letters*, 45, 13240–13248. <https://doi.org/10.1029/2018GL080405>

Badro, J., Siebert, J., & Nimmo, F. (2016). An early geodynamo driven by exsolution of mantle components from Earth's core. *Nature*, 536(7616), 2–328. <https://doi.org/10.1038/nature18594>

Bonomi, M., Bussi, G., Camilloni, C., Tribello, G. A., Banáš, P., Barducci, A., et al. (2019). Promoting transparency and reproducibility in enhanced molecular simulations. *Nature Methods*, 16(8), 670–673. <https://doi.org/10.1038/s41592-019-0506-8>

Boukaré, C. E., Ricard, Y., & Fiquet, G. (2015). Thermodynamics of the MgO–FeO–SiO₂ system up to 140 GPa: Application to the crystallization of Earth's magma ocean. *Journal of Geophysical Research: Solid Earth*, 120(9), 2015JB011929. <https://doi.org/10.1002/2015JB011929>

Davies, C. J., & Greenwood, S. (2023). Dynamics in Earth's core arising from thermo-chemical interactions with the mantle. In *Core–mantle Co-evolution* (pp. 219–258).

Davies, C. J., Pozzo, M., Gubbins, D., & Alfè, D. (2018). Partitioning of oxygen between ferropericlase and Earth's liquid core. *Geophysical Research Letters*, 45(12), 6042–6050. <https://doi.org/10.1029/2018GL077758>

Deng, J. (2024). Large-scale atomistic simulations of magnesium oxide exsolution driven by machine learning potentials: Implications for the early geodynamo. <https://doi.org/10.17605/OSF.IO/MSRV4>

Deng, J., & Du, Z. (2023). Primordial helium extracted from the Earth's core through magnesium oxide exsolution. *Nature Geoscience*, 16(6), 541–545. <https://doi.org/10.1038/s41561-023-01182-7>

Deng, J., Miyazaki, Y., & Lee, K. K. M. (2019). Implications for the melting phase relations in the MgO–FeO system at core–mantle boundary conditions. *Journal of Geophysical Research: Solid Earth*, 124(2), 11–1304. <https://doi.org/10.1029/2018JB015499>

Deng, J., Niu, H., Hu, J., Chen, M., & Stixrude, L. (2023). Melting of MgSiO₃ determined by machine learning potentials. *Physical Review B*, 107(6), 064103. <https://doi.org/10.1103/PhysRevB.107.064103>

Deng, J., & Stixrude, L. (2021a). Deep fractionation of Hf in a solidifying magma ocean and its implications for tungsten isotopic heterogeneities in the mantle. *Earth and Planetary Science Letters*, 562, 116873. <https://doi.org/10.1016/j.epsl.2021.116873>

Deng, J., & Stixrude, L. (2021b). Thermal conductivity of silicate liquid determined by machine learning potentials. *Geophysical Research Letters*, 562, 116873. <https://doi.org/10.1016/j.epsl.2021.116873>

Du, Z., Boujibar, A., Driscoll, P., & Fei, Y. (2019). Experimental constraints on an MgO exsolution-driven geodynamo. *Geophysical Research Letters*, 46(13), 7379–7385. <https://doi.org/10.1029/2019GL083017>

Du, Z., Deng, J., Miyazaki, Y., Mao, H.-k., Karki, B. B., & Lee, K. K. M. (2019). Fate of hydrous Fe-rich silicate melt in Earth's deep mantle. *Geophysical Research Letters*, 46(16), 9466–9473. <https://doi.org/10.1029/2019GL083633>

Du, Z., Jackson, C., Bennett, N., Driscoll, P., Deng, J., Lee, K. K. M., et al. (2017). Insufficient energy from MgO exsolution to power early geodynamo. *Geophysical Research Letters*, 44(22), 11376–11381. <https://doi.org/10.1002/2017GL075283>

Du, Z., & Lee, K. K. M. (2014). High-pressure melting of MgO from (Mg,Fe)O solid solutions. *Geophysical Research Letters*, 41(22), 8061–8066. <https://doi.org/10.1002/2014GL061954>

Fischer, R. A., Campbell, A. J., & Ciesla, F. J. (2017). Sensitivities of Earth's core and mantle compositions to accretion and differentiation processes. *Earth and Planetary Science Letters*, 458, 252–262. <https://doi.org/10.1016/j.epsl.2016.10.025>

Fischer, R. A., Nakajima, Y., Campbell, A. J., Frost, D. J., Harries, D., Langenhorst, F., et al. (2015). High pressure metal–silicate partitioning of Ni, Co, V, Cr, Si, and O. *Geochimica et Cosmochimica Acta*, 167, 177–194. <https://doi.org/10.1016/j.gca.2015.06.026>

Frost, D. A., Avery, M. S., Buffett, B. A., Chidester, B. A., Deng, J., Dorfman, S. M., et al. (2022). Multidisciplinary constraints on the thermal-chemical boundary between Earth's core and mantle. *Geochemistry, Geophysics, Geosystems*, 23(3), e2021GC009764. <https://doi.org/10.1029/2021GC009764>

Frost, D. J., Asahara, Y., Rubie, D. C., Miyajima, N., Dubrovinsky, L. S., Holzapfel, C., et al. (2010). Partitioning of oxygen between the Earth's mantle and core. *Journal of Geophysical Research*, 115(B2), B02202. <https://doi.org/10.1029/2009JB006302>

Helffrich, G., Ballmer, M. D., & Hirose, K. (2018). Core-exsolved SiO_2 dispersal in the Earth's mantle. *Journal of Geophysical Research: Solid Earth*, 123(1), 176–188. <https://doi.org/10.1002/2017JB014865>

Helffrich, G., Hirose, K., & Nomura, R. (2020). Thermodynamical modeling of liquid Fe-Si-Mg-O:molten magnesium silicate Release from the core. *Geophysical Research Letters*, 47(21), e2020GL089218. <https://doi.org/10.1029/2020GL089218>

Hirose, K., Morard, G., Sinnjo, R., Umemoto, K., Hernlund, J., Helffrich, G., & Labrosse, S. (2017). Crystallization of silicon dioxide and compositional evolution of the Earth's core. *Nature*, 543(7643), 4–102. <https://doi.org/10.1038/nature21367>

Hirose, K., Wood, B., & Vočadlo, L. (2021). Light elements in the Earth's core. *Nature Reviews Earth and Environment*, 2(9), 645–658. <https://doi.org/10.1038/s43017-021-00203-6>

Holmström, E., & Stixrude, L. (2015). Spin crossover in ferropericlase from first-principles molecular dynamics. *Physical Review Letters*, 114(11), 117202. <https://doi.org/10.1103/physrevlett.114.117202>

Hoover, W. G. (1985). Canonical dynamics: Equilibrium phase-space distributions. *Physical Review A*, 31(3), 1695–1697. <https://doi.org/10.1103/PhysRevA.31.1695>

Hornik, K., Stinchcombe, M., & White, H. (1989). Multilayer feedforward networks are universal approximators. *Neural Networks*, 2(5), 359–366. [https://doi.org/10.1016/0893-6080\(89\)90020-8](https://doi.org/10.1016/0893-6080(89)90020-8)

Karki, B. B., Ghosh, D. B., Maharan, C., Karato, S.-i., & Park, J. (2018). Density-pressure profiles of Fe-bearing MgSiO_3 liquid: Effects of valence and Spin states, and implications for the chemical evolution of the lower mantle. *Geophysical Research Letters*, 45(9), 3959–3966. <https://doi.org/10.1029/2018GL077149>

Karki, B. B., & Khanduja, G. (2006). Vacancy defects in MgO at high pressure. *American Mineralogist*, 91(4), 511–516. <https://doi.org/10.2138/am.2006.1998>

Korell, J.-A., French, M., Steinle-Neumann, G., & Redmer, R. (2019). Paramagnetic-to-Diamagnetic transition in dense liquid iron and its influence on electronic transport properties. *Physical Review Letters*, 122(8), 086601. <https://doi.org/10.1103/PhysRevLett.122.086601>

Kresse, G., & Furthmüller, J. (1996). Efficiency of ab-initio total energy calculations for metals and semiconductors using a plane-wave basis set. *Computational Materials Science*, 6(1), 15–50. [https://doi.org/10.1016/0927-0256\(96\)00008-0](https://doi.org/10.1016/0927-0256(96)00008-0)

Kresse, G., & Joubert, D. (1999). From ultrasoft pseudopotentials to the projector augmented-wave method. *Physical Review B*, 59(3), 1758–1775. <https://doi.org/10.1103/PhysRevB.59.1758>

Liu, W., Zhang, Y., Yin, Q.-Z., Zhao, Y., & Zhang, Z. (2019). Magnesium partitioning between silicate melt and liquid iron using first-principles molecular dynamics: Implications for the early thermal history of the Earth's core. *Earth and Planetary Science Letters*, 531, 115934. <https://doi.org/10.1016/j.epsl.2019.115934>

Lorenz, S., Grob, A., & Scheffler, M. (2004). Representing high-dimensional potential-energy surfaces for reactions at surfaces by neural networks. *Chemical Physics Letters*, 395(4–6), 210–215. <https://doi.org/10.1016/j.cplett.2004.07.076>

Ma, Z. T. (2001). Thermodynamic description for concentrated metallic solutions using interaction parameters. *Metallurgical and Materials Transactions B, Process Metallurgy and Materials Processing Science*, 32(1), 87–103. <https://doi.org/10.1007/s11663-001-0011-0>

Mermin, N. D. (1965). Thermal properties of the inhomogeneous electron gas. *Physical Review*, 137(5A), A1441–A1443. <https://doi.org/10.1103/PhysRev.137.A1441>

Mittal, T., Knezeck, N., Arveson, S. M., McGuire, C. P., Williams, C. D., Jones, T. D., & Li, J. (2020). Precipitation of multiple light elements to power Earth's early dynamo. *Earth and Planetary Science Letters*, 532, 116030. <https://doi.org/10.1016/j.epsl.2019.116030>

Nimmo, F. (2015). 8.02 – energetics of the core. In G. Schubert (Ed.), *Treatise on geophysics* (2nd ed., pp. 27–55). Elsevier.

Okuda, Y., Hirose, K., Ohta, K., Kawaguchi-Imada, S., & Oka, K. (2024). Electrical conductivity of dense MgSiO_3 melt under static compression. *Geophysical Research Letters*, 51(12), e2024GL109741. <https://doi.org/10.1029/2024GL109741>

O'Rourke, J. G., & Stevenson, D. J. (2016). Powering Earth's dynamo with magnesium precipitation from the core. *Nature*, 529(7586), 387–389. <https://doi.org/10.1038/nature16495>

Osawa, H., Hirose, K., Mitome, M., Bando, Y., Sata, N., & Ohishi, Y. (2008). Chemical equilibrium between ferropericlase and molten iron to 134 GPa and implications for iron content at the bottom of the mantle. *Geophysical Research Letters*, 35(5). <https://doi.org/10.1029/2007GL032648>

Peng, Y., & Deng, J. (2024). Hydrogen diffusion in the lower mantle revealed by machine learning potentials. *Journal of Geophysical Research: Solid Earth*, 129(4), e2023JB028333. <https://doi.org/10.1029/2023JB028333>

Perdew, J. P., Ruzsinszky, A., Csonka, G. I., Vydrov, O. A., Scuseria, G. E., Constantin, L. A., et al. (2008). Restoring the density-gradient expansion for exchange in solids and surfaces. *Physical Review Letters*, 100(13), 136406. <https://doi.org/10.1103/PhysRevLett.100.136406>

Piaggi, P. M., & Parrinello, M. (2019). Multithermal-multibaric molecular simulations from a variational principle. *Physical Review Letters*, 122(5), 050601. <https://doi.org/10.1103/PhysRevLett.122.050601>

Plimpton, S. J., Kohlmeyer, A., Thompson, A. P., Moore, S. G., & Berger, R. (2022). Lammps: Large-Scale atomic/molecular massively parallel simulator. *Zenodo*. Retrieved from <https://zenodo.org/record/10806836>

Rubie, D. C., Jacobson, S. A., Morbidelli, A., O'Brien, D. P., Young, E. D., de Vries, J., et al. (2015). Accretion and differentiation of the terrestrial planets with implications for the compositions of early-formed Solar System bodies and accretion of water. *Icarus*, 248, 89–108. <https://doi.org/10.1016/j.icarus.2014.10.015>

Scipioni, R., Stixrude, L., & Desjarlais, M. P. (2017). Electrical conductivity of SiO_2 at extreme conditions and planetary dynamos. *Proceedings of the National Academy of Sciences*, 114(34), 9009–9013. <https://doi.org/10.1073/pnas.1704762114>

Sega, M., Hantal, G., Fábián, B., & Jedlovszky, P. (2018). Pytim: A python package for the interfacial analysis of molecular simulations. *Journal of Computational Chemistry*, 39(25), 2118–2125. <https://doi.org/10.1002/jcc.25384>

Stixrude, L., Scipioni, R., & Desjarlais, M. P. (2020). A silicate dynamo in the early Earth. *Nature Communications*, 11(1), 935. <https://doi.org/10.1038/s41467-020-14773-4>

Tarduno, J. A., Cottrell, R. D., Davis, W. J., Nimmo, F., & Bono, R. K., (2015). A Hadean to Paleoarchean geodynamo recorded by single zircon crystals. *Science*, 349(6247), 521–524. <https://doi.org/10.1126/science.aaa9114>

Tarduno, J. A., Cottrell, R. D., Watkeys, M. K., Hofmann, A., Doubrovine, P. V., Mamajek, E. E., et al., (2010). Geodynamo, solar Wind, and magnetopause 3.4 to 3.45 billion years ago. *Science*, 327(5970), 1238–1240. <https://doi.org/10.1126/science.1183445>

Van Orman, J. A., Fei, Y. W., Hauri, E. H., & Wang, J. H. (2003). Diffusion in MgO at high pressures: Constraints on deformation mechanisms and chemical transport at the core-mantle boundary. *Geophysical Research Letters*, 30(2), 1056. <https://doi.org/10.1029/2002gl016343>

Wahl, S. M., & Militzer, B. (2015). High-temperature miscibility of iron and rock during terrestrial planet formation. *Earth and Planetary Science Letters*, 410, 25–33. <https://doi.org/10.1016/j.epsl.2014.11.014>

Wang, H., Zhang, L., Han, J., & Weinan, E. (2018). DeePMD-kit: A deep learning package for many-body potential energy representation and molecular dynamics. *Computer Physics Communications*, 228, 178–184. <https://doi.org/10.1016/j.cpc.2018.03.016>

Willard, A. P., & Chandler, D. (2010). Instantaneous liquid interfaces. *The Journal of Physical Chemistry B*, 114(5), 1954–1958. <https://doi.org/10.1021/jp909219k>

Wilson, A. J., Pozzo, M., Davies, C. J., Walker, A. M., & Alfè, D. (2023). Examining the power supplied to Earth's dynamo by magnesium precipitation and radiogenic heat production. *Physics of the Earth and Planetary Interiors*, 343, 107073. <https://doi.org/10.1016/j.pepi.2023.107073>

Xiao, B., & Stixrude, L. (2018). Critical vaporization of MgSiO₃. *Proceedings of the National Academy of Sciences*, 115(21), 5371–5376. <https://doi.org/10.1073/pnas.1719134115>

Zeng, J., Zhang, D., Lu, D., Mo, P., Li, Z., Chen, Y., et al. (2023). DeePMD-kit v2: A software package for deep potential models. *The Journal of Chemical Physics*, 159(5), 054801. <https://doi.org/10.1063/5.0155600>

Zhang, L., Han, J., Wang, H., Car, R., & E, W. (2018). Deep potential molecular dynamics: A scalable model with the accuracy of Quantum mechanics. *Physical Review Letters*, 120(14), 143001. <https://doi.org/10.1103/PhysRevLett.120.143001>